




Strathprints Institutional Repository

Apneseth, Claus Christian and Day, Alexander and Clelland, David (2010) *Hydrodynamics of an oscillating articulated eel-like structure*. *Ocean Engineering*, 37 (13). pp. 1221-1232. ISSN 0029-8018

Strathprints is designed to allow users to access the research output of the University of Strathclyde. Copyright © and Moral Rights for the papers on this site are retained by the individual authors and/or other copyright owners. You may not engage in further distribution of the material for any profitmaking activities or any commercial gain. You may freely distribute both the url (<http://strathprints.strath.ac.uk/>) and the content of this paper for research or study, educational, or not-for-profit purposes without prior permission or charge.

Any correspondence concerning this service should be sent to Strathprints administrator: <mailto:strathprints@strath.ac.uk>

AUTHOR QUERY FORM

 ELSEVIER	Journal: OE Article Number: 1820	Please e-mail or fax your responses and any corrections to: E-mail: corrections.essd@elsevier.macipd.com Fax: +44 1392 285878
--	---	--

Dear Author,

Any queries or remarks that have arisen during the processing of your manuscript are listed below and highlighted by flags in the proof. Please check your proof carefully and mark all corrections at the appropriate place in the proof (e.g., by using on-screen annotation in the PDF file) or compile them in a separate list.

For correction or revision of any artwork, please consult <http://www.elsevier.com/artworkinstructions>.

Articles in Special Issues: Please ensure that the words ‘this issue’ are added (in the list and text) to any references to other articles in this Special Issue

Uncited references: References that occur in the reference list but not in the text – please position each reference in the text or delete it from the list.	
Missing references: References listed below were noted in the text but are missing from the reference list – please make the list complete or remove the references from the text.	
Location in article	Query/remark Please insert your reply or correction at the corresponding line in the proof
Q1	A slight change has been made to the sentence “this study examines...segments oscillating”. Please check the same for correctness.

Electronic file usage

Sometimes we are unable to process the electronic file of your article and/or artwork. If this is the case, we have proceeded by:

Scanning (parts of) your article Rekeying (parts of) your article Scanning the artwork

Thank you for your assistance.



Contents lists available at ScienceDirect

Ocean Engineering

journal homepage: www.elsevier.com/locate/oceaneng

Hydrodynamics of an oscillating articulated eel-like structure

C.C. Apneseth^a, A.H. Day^{b,*}, D. Clelland^b^a Miko Marine AS, Ruseeløkkveien 26, PO Box 1534 – Vika, N-0117 Oslo, Norway^b Department of Naval Architecture and Marine Engineering, University of Strathclyde, Glasgow, Scotland, UK

ARTICLE INFO

Article history:

Received 10 November 2009

Accepted 1 June 2010

Keywords:

Hydrodynamics

Fish locomotion

Swimming

Model testing

ABSTRACT

This study examines the hydrodynamic performance of a highly simplified eel-like structure consisting of three articulated segments with the two aft segments oscillating. A physical model was built and tested to determine the forces developed with the model stationary, to find the self-propulsion speed, and to explore the effect on hydrodynamic performance of different swimming patterns. It was found that hydrodynamic performance increases with increasing oscillation frequency; the highest forces when stationary, and the highest self-propulsion speeds were produced by swimming patterns in which the amplitude in the aft segment is larger than that in the forward segment, and in which the motion of the aft segment lags the forward segment.

A simple semi-empirical model based on Morison's equation was implemented to predict the hydrodynamic forces. This was shown to predict mean thrust well in cases in which the aft segment oscillates in phase with the forward segment, but less reliably when the phase difference between the segments increases. Force time histories are generally not well-predicted using this approach. Nonetheless, self-propulsion speeds are predicted within 30% in all cases examined.

© 2010 Published by Elsevier Ltd.

1. Introduction

1.1. Background

The hydrodynamics of fish propulsion has been a subject of theoretical interest for many years. More than eighty years ago, Breder (1926) made an early attempt at the classification of methods of aquatic propulsion. Gawn (1950) described the relevance of fish propulsion to naval architects. One of the key studies of these phenomena was made by Lighthill (1960), whose work apparently started in investigating the well-known idea known as “Gray's Paradox”, (Gray, 1936), which suggested that dolphins swim many times faster than their muscle mass should allow them.

In recent years, interest in this area has expanded, as the possibilities for practical application have grown, particularly with the development of low-cost robotic technologies. Notable contributions have been made by Videler (1993), Azuma (2006), and the work of the MIT team led by Triantafyllou who have developed the “Robotuna” over a fifteen year period (see for example Triantafyllou et al. 1996, 2002). A number of recent studies have addressed the issues of fish propulsion specifically in the context of the challenges of autonomous fish-like vehicles, and as such, a significant body of work has concentrated on the control algorithms required for these vehicles, such as the studies

of McIsaac and Ostrowski (2003). Particular advantages perceived include the potential for improved acceleration and/or manoeuvrability and the ability to operate in environments in which conventional propellers may become entangled.

Many of the robotic fish studied have attempted to replicate fish kinematics in a realistic or semi-realistic manner and have thus utilized relatively large numbers of segments distributed along the “spine” of the vehicle in order to generate the realistic motion. These can provide valuable insight into the hydrodynamics of fish propulsion, but may prove difficult to implement on larger practical devices or vehicles.

1.2. Aims and objectives of current study

In contrast, the aim of the current study was to examine the hydrodynamics of highly simplified eel-like structures consisting of a small number of relatively large segments and then to explore the feasibility of predicting the hydrodynamic performance of these structures using simple models based on well-known semi-empirical formulations such as the “Morison Equation”.

The first objective of the study was to design and build a simplified physical model of such a structure and test it in a towing tank. The model was built in a modular fashion to allow segments to be added in sequence, to allow the hydrodynamics to be explored for different numbers of segments. In the current study, physical models with two and three segments are described.

In parallel, the second objective was to develop a simplified approach to the prediction of hydrodynamic forces, based on a

* Corresponding author. Tel.: +44 141 548 3303; fax: +44 141 552 2879
E-mail address: sandy.day@strath.ac.uk (A.H. Day).

Morison-like approach, to investigate the possibility of developing a rapid semi-empirical method which could be used to predict global parameters of the structure at the preliminary design stage. The validity of the approach developed would be explored by attempting to predict the forces generated by the model at zero speed and the self-propulsion speed of the swimming model, and by comparing with the data determined from the tank tests.

2. Kinematics of a simplified articulated eel-like structure

Before developing a physical model of a simplified eel-like structure, it is important to understand the kinematics of the simplified model eel and how these relate to the kinematics of real eels. Fish locomotion was classified by Breder (1926) as being ostraciiform, carangiform or anguilliform depending upon how much of a “wavelength” of motion was exhibited in the fish body. Ostraciiform locomotion is used by fish with relatively inflexible bodies, which use their caudal (tail) fin for propulsion. Carangiform locomotion involves the posterior part of the fish body flexing to create undulations, which can be viewed as being of approximately one half a wavelength; this is the mode used by faster swimming fish such as tuna, mackerel and marlin. Eels on the other hand are flexible throughout their length and flex with undulations of more than half a wavelength; this is described as anguilliform locomotion (see Fig. 1). Subsequent researchers have indicated that this classification is an over-simplification of the variation between real fish, but the terms are still widely used.

The kinematics of a robotic eel depends upon a number of variables, including the number of segments, the length of the segments, the motion of the head of the eel relative to the water, the amplitude and frequency of oscillation in the various joints, and the phase angle between oscillations in the joints.

In nature, an eel swimming in a straight line at low to moderate speeds will have minimal head movement in the lateral plane, and will swim with a backwards travelling wave, which can reasonably be idealized as a sinusoid of linearly increasing amplitude toward the tail (Gillis, 1998). Since the current study

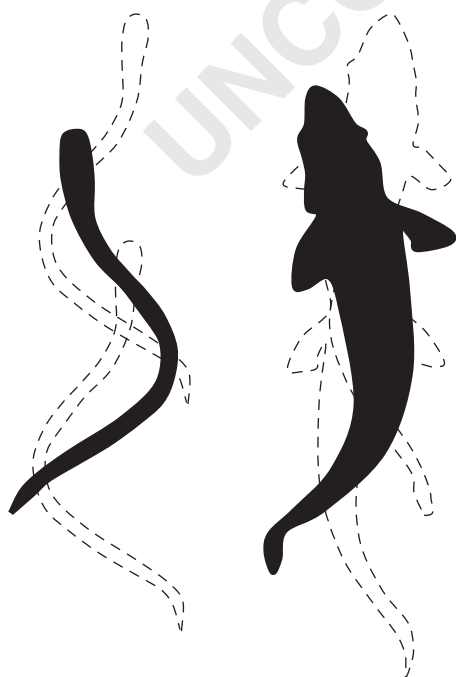


Fig. 1. Anguilliform locomotion (left) and Carangiform locomotion (right) (from Gray, 1936)

dealt exclusively with motion in the horizontal plane, it was considered reasonable to fix the head of the model eel to the towing carriage in the test tank.

The discretisation of the simplified structure is illustrated in Fig. 2 showing four moving segments. The continuous line represents the idealized motion at an arbitrary point in time. As the amplitude of oscillation increases towards the tail, the angular displacement also increases. With the moderate number of sections adopted here, it could be argued that an unequal distribution of length of the sections should be adopted to allow the most accurate fit to such a curve; however in the current study it was decided that the lengths of the moving sections would be kept uniform in the interests of standardization.

The motion of the simplified eel can then be described in terms of two variables for each moving segment: the amplitude of motion and the phase of the motion relative to the segment immediately in front of it. Two further global variables are required: the frequency of oscillation and the forward speed. In principle the frequency of oscillation could be allowed to vary between segments; however this would lead to time-varying motion patterns which are not observed in nature for steady propulsion. A more subtle point relates to the form of the oscillation: it is not necessarily obvious that the motion of each segment should be exactly sinusoidal in order for the instantaneous profile to follow the idealized form described. However, for the current study, the motions were constrained to be sinusoidal.

The kinematics of a segmented eel can be considered in a straightforward manner. The geometry of the system is shown in Fig. 3. The origin of the co-ordinate system is located at the leading edge of the first moving segment. The eel is swimming from right to left in this system.

The location of the end points of the segments in the global co-ordinate system (X, Y) is given as

$$\begin{aligned} X_i &= X_{i-1} + L_{i-1} \cos \theta_{i-1} & \text{with } X_1 &= 0 \\ Y_i &= Y_{i-1} + L_{i-1} \sin \theta_{i-1} & \text{with } Y_1 &= 0 \end{aligned} \quad (1)$$

Hence the velocity of the end points is

$$\begin{aligned} \dot{X}_i &= \dot{X}_{i-1} - \dot{\theta}_{i-1} L_{i-1} \sin \theta_{i-1} & \text{with } \dot{X}_1 &= U \\ \dot{Y}_i &= \dot{Y}_{i-1} + \dot{\theta}_{i-1} L_{i-1} \cos \theta_{i-1} & \text{with } \dot{Y}_1 &= 0 \end{aligned} \quad (2)$$

where U is the speed of the eel (positive left to right); the acceleration of the end points is

$$\begin{aligned} \ddot{X}_i &= \ddot{X}_{i-1} - \ddot{\theta}_{i-1} L_{i-1} \cos \theta_{i-1} - \dot{\theta}_{i-1}^2 L_{i-1} \sin \theta_{i-1} & \text{with } \ddot{X}_1 &= 0 \\ \ddot{Y}_i &= \ddot{Y}_{i-1} - \ddot{\theta}_{i-1} L_{i-1} \sin \theta_{i-1} + \dot{\theta}_{i-1}^2 L_{i-1} \cos \theta_{i-1} & \text{with } \ddot{Y}_1 &= 0 \end{aligned} \quad (3)$$

Velocities and acceleration at intermediate points in a segment may be found from appropriately weighted sums of the values at the end points.

We now consider the velocity and acceleration distributions for a three segment (two moving) eel. In the very simplest case, the eel is not moving forwards and two segments move in phase with each other and with the same amplitude. If the amplitude of the angular displacement is 30 degrees, this case can be designated as 30-30-0, indicating the amplitude of angular motion of each segment and the relative phase lag of segment 2

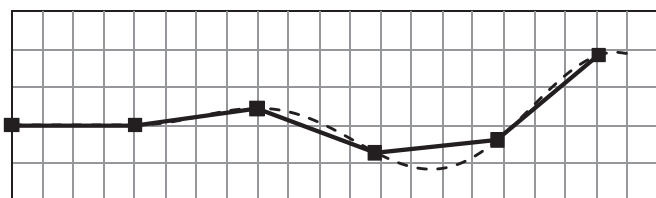


Fig. 2. Discretisation of a simplified articulated eel.

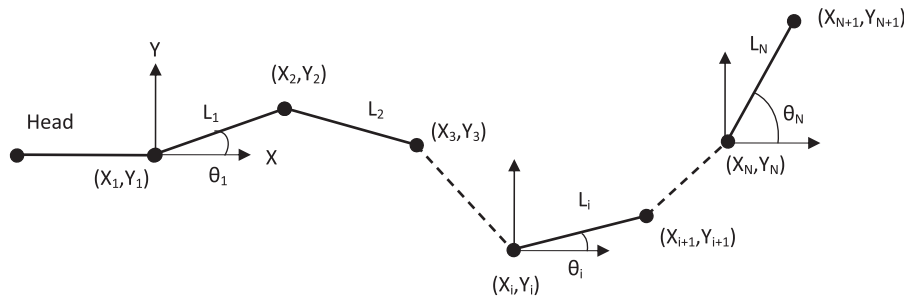


Fig. 3. Geometry of an articulated eel.

with respect to segment 1. In this case the motion is extremely simple; the velocity in this case is always perpendicular to the segment (except when zero); however the acceleration is only perpendicular to the segment when the velocity is zero, i.e. when the displacement is maximum.

A swimming pattern closer to the real eel has a backwards travelling wave with amplitude increasing towards the tail. In order to achieve this, the amplitude of segment 2 must be greater than that of segment 1 and the phase of segment 2 must lag segment 1. Fig. 4 shows the 30-40-60 case (using the same notation) with zero forward speed. In this scenario, neither the acceleration nor velocity is normal to the segments, except for the velocity on the forward segment. The final plot of Fig. 4 shows the instantaneous positions of the second segment in this case, and the path followed by the tip of the tail. This is no longer a circular arc, instead it forms a curved figure-of-eight.

The two previous cases both illustrate velocity and acceleration with the mean forward velocity equal to zero; this is equivalent to a “bollard-pull” condition in naval architecture terms and forms the initial condition when the structure sets off from rest. With a mean forward speed, the velocity distribution is more complex, as illustrated in Fig. 5, which shows the velocity for a forward speed of 0.1 m/s.

3. A simple hydrodynamic model of an oscillating articulated structure

A wide range of approaches have been attempted for modelling of fish-like locomotion. At the simplest end, some authors have done calculations based simply on cross-flow drag coefficients (e.g. McIsaac and Ostrowski, 2003). Such an approach entirely ignores inertial forces. Given that the kinematics have been shown to lead to reasonably complex acceleration patterns, it seems unlikely that a method which entirely neglects forces related to fluid acceleration will produce reliable results.

A range of potential-flow methods have been developed based on solution of analytical equations. Well-known examples include the “elongated-body theory” developed by Lighthill (1960) and the “large-amplitude elongated-body theory” (Lighthill, 1971). There are two key problems in applying these types of slender-body approach to the articulated eel. Firstly, in some cases, the approaches are linearized, in the sense that the amplitudes of oscillation are considered small with respect to the length, thus the slopes of the segments relative to the mean direction of motion are also assumed to be small. In the cases examined here, the segment slopes are as high as 40 degrees, which cannot reasonably be considered small. Secondly, these types of approach are generally designed to reflect the kinematics of real fish; as such, they are intended to model smoothly curving bodies, in which the slope varies in a continuous fashion along the length, at any given moment in time. In contrast, the articulated eel exhibits

constant slope along each segment and discontinuities in slope at each hinge. These methods could arguably be applied in an approximate fashion to an articulated eel with many segments, in which the discontinuities at each hinge would be reasonably small, by essentially curve-fitting the centreline of the segments in some suitable manner. However, with a small number of segments, as adopted here, the articulated eel exhibits substantial discontinuities in slope at each hinge and thus these methods would not be expected to produce reliable results.

In recent years a number of computational solutions have also been implemented. These have been based on both potential-flow computations, using approaches such as the vortex-lattice method (e.g. Singh and Pedley, 2008) and CFD-based computations (e.g. Carling et al., 1998). Computational approaches are clearly valuable for analysis of mature designs; however CFD methods in particular are less well-suited to preliminary design studies due to the large human and computer resources required to develop a mesh and solve the flow field.

One of the aims of the current study was to investigate the extent to which the performance of a simplified oscillating articulated structure could be modelled using a simple semi-empirical engineering approach, rather than using a complex full-field flow solver. If such an approach gave reliable predictions it could potentially be extremely valuable in the preliminary design of a real structure and the optimization of its swimming pattern and control. It was felt unlikely from the outset that it would be possible to generate such a model without having some experimental data which would allow the calculation of suitable flow force coefficients; however, if data from a small set of tests could be used in conjunction with a simple model to predict performance over a wide range of geometric variations and/or swimming patterns, there would be potential for some significant advantages to the designer.

The Morison equation (Morison et al., 1950) is widely used for quick and simple calculations in offshore engineering, such as those in preliminary design. Originally developed for predicting wave load on a fixed vertical pile, it has since been used to predict forces on an enormous range of structures oriented at different angles to the flow, moving in still water, or moving in a flow field. In the current problem, the Morison equation can be easily applied to one segment of the articulated eel by integration of the velocity and acceleration, normal to the segment in the plane of the motion. Numerical integration is convenient for handling discontinuities, for example in mass distributions, and is adopted here.

Each segment is divided into M elements; the force on each element can then be written as

$$f_{x,i,j} = \frac{\pi D_i^2}{8} C_{a,i,j} \rho \frac{L_i}{M} \ddot{X}_{ij}^\perp + D_i C_{d,i,j} \rho \frac{L_i}{M} \dot{X}_{ij}^\perp |V_{ij}^\perp| + m_{ij} \ddot{X}_{ij} \quad (4)$$

$$f_{y,i,j} = \frac{\pi D_i^2}{8} C_{a,i,j} \rho \frac{L_i}{M} \ddot{Y}_{ij}^\perp + D_i C_{d,i,j} \rho \frac{L_i}{M} \dot{Y}_{ij}^\perp |V_{ij}^\perp| + m_{ij} \ddot{Y}_{ij} \quad (5)$$

where the subscript i, j indicates the value appropriate to the j th element of the i th segment.

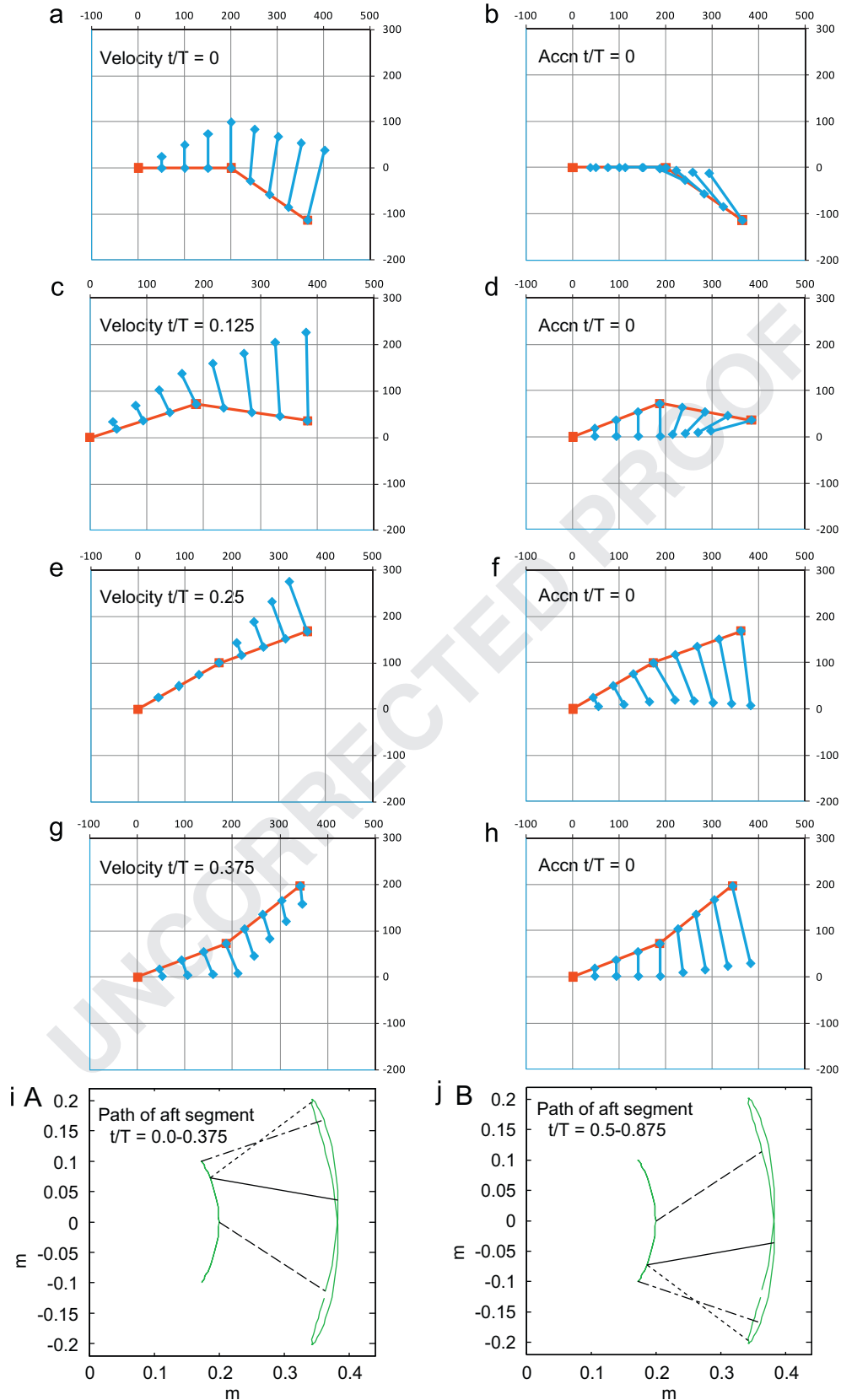


Fig. 4. Velocity, acceleration, and path of segment 2 for 30-40-60 case with zero forward speed.

Here V_{ij}^\perp is the component of velocity normal to the element; $\dot{X}_{ij}^\perp, \dot{Y}_{ij}^\perp, \ddot{X}_{ij}^\perp$ and \ddot{Y}_{ij}^\perp are the components of the normal velocity and acceleration parallel to the X and Y axes, respectively. The

contributions of the tangential velocities and accelerations to the hydrodynamic forces are considered negligible. The first term in each equation is the resolved Morison inertia force; $C_{a,ij}$ is the

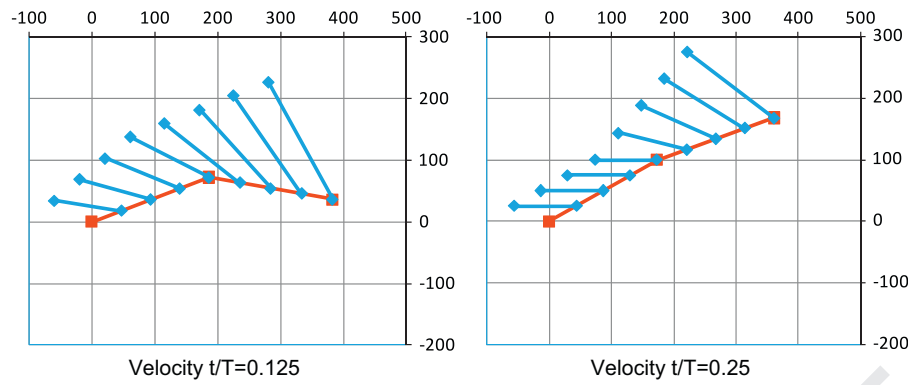


Fig. 5. Velocity for 30-40-60 case with forward speed.

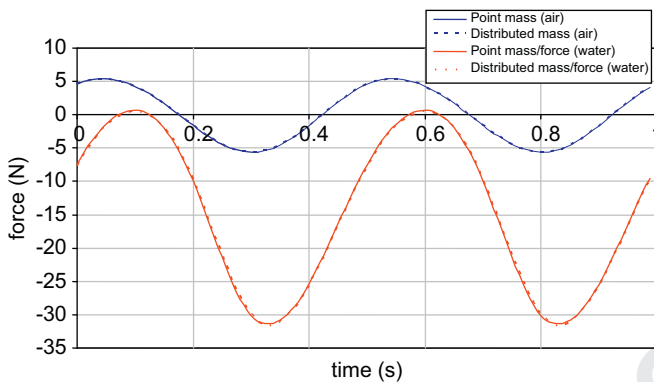


Fig. 6. Time history of longitudinal force for assumed values.

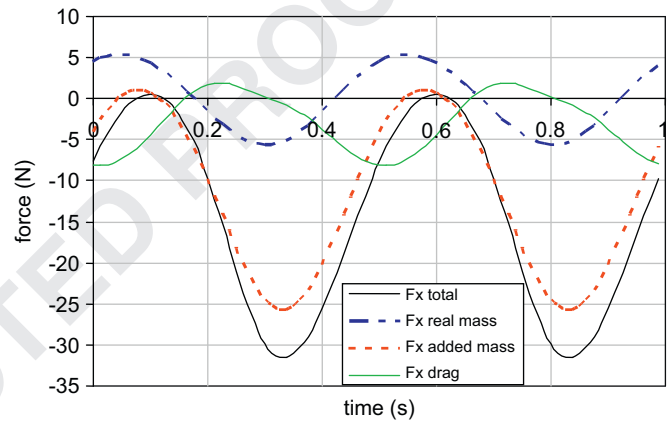


Fig. 7. Time history of longitudinal force components for assumed values.

section added mass coefficient for the j th element of the i th segment (non-dimensionalised with respect to a circular cylinder of diameter equal to the vertical height of the eel cross-section D_i). The second term is the resolved Morison drag force; $C_{d,i,j}$ is the corresponding section drag coefficient. The third term is the force related to solid inertia. The instantaneous thrust may be found as the sum overall elements of all segments of the longitudinal forces

$$T(t) = \sum_{i=1}^N \sum_{j=1}^M f_{x,i,j} \quad (6)$$

and the mean thrust can be obtained by integrating this over a whole cycle of motion. Clearly this approach makes some substantial approximations about the flow field and the mass distribution of the eel.

Some sample calculations were carried out using this highly simplified model in order to examine the predictions of forward and transverse forces. These were based on assumed values of hydrodynamic force coefficients.

Fig. 6 shows the time histories of the total longitudinal force based on an assumption that the two moving segments have a mass of 2 kg, length of 200 mm, and depth of 200 mm and that the eel is swimming in the 30-40-60 pattern at zero forward speed. In each case the calculations are carried out for oscillations in air, assuming that hydrodynamic forces are negligible, and in water, for which it was assumed that $C_a=1$, $C_d=1.2$. Furthermore, in order to explore the sensitivity of the result to the distribution of mass, velocity and acceleration properties, the calculations were also carried out using a “lumped mass” approach in which velocities, accelerations, and forces are calculated only each segment midpoint. It can be seen that in this case there is no great difference between the two approaches to discretisation in

the prediction of the longitudinal force. It can also be seen that the model does predict a net thrust—i.e. a mean force in the negative X-direction. Fig. 7 shows the breakdown of this force into the components corresponding to the three terms of Eq. (4).

4. Design and implementation of model experiment

4.1. Model design

A working model of the simplified eel was built in order to explore these ideas further. The engineering of the model eel is by no means straightforward and the final version was quite different in a number of respects from the original versions. It was decided early in the study to concentrate on a three segment model, with the forward segment attached to the towing carriage and two moveable segments behind it.

One of the main challenges was the drive system; in the early versions, the segments were driven through a pair of wire drives, with the motors mounted on the carriage and the wires passing through the sting into the eel; however after a lot of effort this was abandoned as it proved impossible to achieve the desired degree of control of the motions. The major problem in this regard proved to be the elasticity of the wires. These had to be relatively flexible to work reliably with the relatively small sheaves in the numerous pulleys; however this requirement then precluded the use of wire, which was stiff in tension. Given the length of wire required, it was calculated that movement of one typical oscillation amplitude from the centre to one side could be achieved by a 2% extension in the wire with the motor stationary. Various attempts were made to address this problem by

pre-tensioning the wire, but these solutions led to more challenges as the increased tension induced more frictional loading; eventually this idea was abandoned.

The version tested used a pair of shaft drives passing through the sting connected to a set of toothed timing belts to transmit the motion to the moving segments. The sting was mounted on a substantial plate above the water, which provided a rigid base for the motors. The motors then drove the shaft via a timing belt. The toothed wheels on the motor and shaft were markedly different in size in order to behave like a gearbox. The entire system was then mounted on a six-component load cell.

The segments were constructed from aluminium with rectangular cross-sections. The aft-most segment was tapered to a point in both vertical and transverse directions. A 50 mm high fin ran along the centre plane of the upper and lower surfaces. Unfortunately, due to the many design changes through the study, in the final version it did not prove possible to retain solid sides throughout the main body as these impeded the timing belts with larger motions. Consequently some openings were left in the main body. However, a small set of tests carried out with the openings sealed showed that the effect of flow through the openings reduced the mean thrust by less than 2%. The sting was also constructed from aluminium with triangular fairings fore and aft. A photograph and a schematic drawing of the eel and sting are shown in Fig. 8.

4.2. Instrumentation and control

The motors were controlled using a closed-loop position control system utilising tachometers on the motors as well as potentiometers mounted on the motor shaft. The command signals for the motor drives were generated using a D/A converter. The measured data, sampled on a 12-bit A/D converter, consisted of the potentiometer signals indicating the instantaneous positions of the eel segments, the speed of the carriage and the forces and moments. The three force/moment components in the horizontal plane were also recorded.

It was originally intended to estimate the input power from the electrical demand on the motors. This could then be used to calculate the propulsive efficiency using the measured global forces and velocities. Unfortunately, the measurements were dominated by effects related to the relatively low efficiency of the transmission system, and reliable results could not be obtained

within the constraints of the study. As a consequence, these measurements were discarded.

4.3. Signal conditioning and correction

One weakness of the design was the siting of the potentiometers on the motor shaft. This was driven by budget constraints; however the corollary was that it was difficult to verify that dynamic effects due to response of the shafts and timing belt system did not lead to dynamic errors in angular measurement. In order to quantify these effects, a complete set of tests were carried out in air. From a knowledge of the measured force in X and Y directions and an assumption that the first two terms in Eq. (4) are zero in air, it is possible to infer a phase correction which minimizes the error between the computed and measured force signals in X and Y directions for each test. This correction was found to increase with increasing frequency and with decreasing amplitude. Typical value was around 1 degree; the largest value found was 3.6 degrees. The data from these tests was also used to identify the time-history of force resulting from the solid inertia of the eel. This time history could then be subtracted from the corresponding time-history of total measured force found from the tests in water in order to isolate the hydrodynamic forces.

Due to the complex motion of the eel itself, the eel drive system, and the motion of the carriage, there were a variety of sources of mechanical noise in the system, as well as some well-defined structural vibration frequencies. Fortunately, Fourier analysis showed that the majority of the noise occurred at frequencies around an order of magnitude above the oscillation frequencies of the eel. In order to remove these noise sources from the signal, an approach was adopted employing Fourier reconstruction of the signals based on the harmonics of the oscillation frequency. This was utilized in examining the time histories of the force signal; however it should be pointed out that since the noise has a zero mean, the time-averaged thrust was taken from an integer number of oscillation-frequency cycles of the raw data. The complete data processing procedure is illustrated in Fig. 9.

Since the sting is quite substantial and the load cell used to measure the towing force is located above the sting, it is important to correct the measured force for the drag of the sting. This was achieved in an approximate manner by building an exact replica of the sting and towing over a range of speeds. A polynomial fit was then applied to the data in order to allow the sting resistance to be carried out at any speed within the range. It was found that the resistance of the sting was rather higher than the frictional resistance (as calculated from the ITTC 1957 friction line with a form factor of unity), suggesting that there is some wave-making and viscous pressure resistance as well as friction.

This approach is imperfect for two reasons. Firstly it ignores hydrodynamic interaction between the sting and eel; secondly it neglects the effect of the wetted area of the end of the sting (and the corresponding area on the eel covered by the sting) as well as any resistance related to flow around the end of the sting. It is therefore likely that the sting resistance is over-estimated. Nonetheless, it was not possible to improve on this approach within the constraints of the project.

5. Model testing program and results

Three main series of tests were carried out with the model in the towing tank at the Kelvin Hydrodynamics Laboratory ($76 \times 4.6 \times 2.5 \text{ m}^3$). In the first set of tests the two moving segments were controlled to move in unison – i.e. with the same

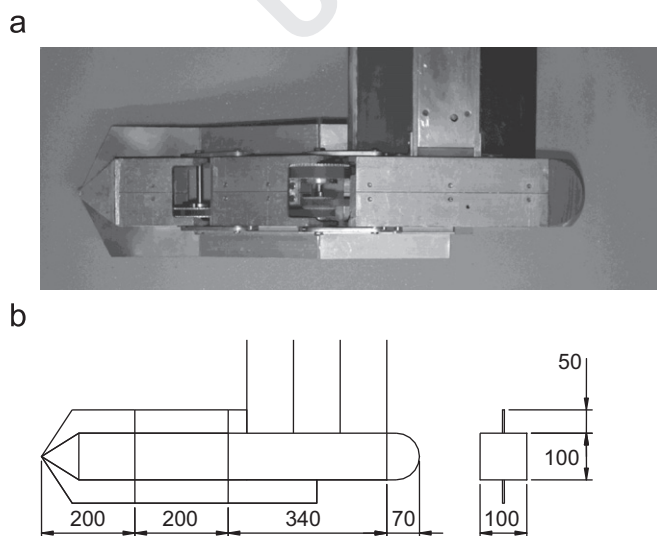


Fig. 8. Final version of model eel: (a) model Eel mounted on sting and (b) schematic diagram of Model Eel.

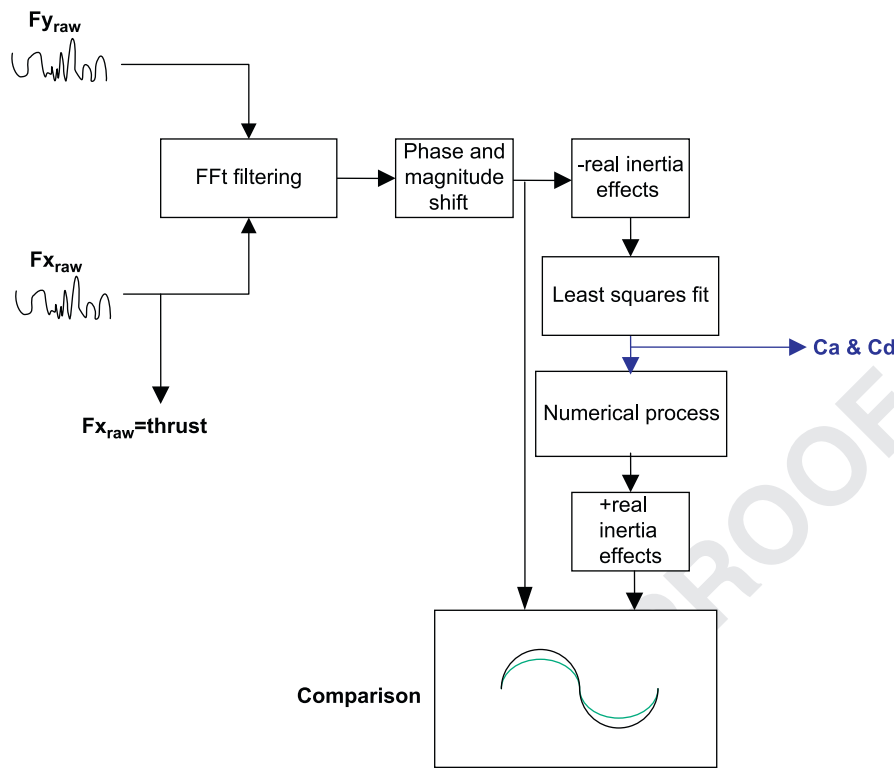


Fig. 9. Data processing block diagram.

oscillation amplitude and with zero phase difference. In this case the two segments act as if they are rigidly joined. These tests were conducted with zero forward speed. This type of test was described as a “single flapper”. The second set of tests retained the zero forward speed condition, but adopted more realistic swimming patterns, with larger amplitude in the aft segment and a phase difference between the two motions. This was described as a “double-flapper” test. The third and final set of tests included the effect of forward speed. These tests were carried out over a range of speeds in order to determine the self-propulsion point.

It should be pointed out that these tests are not directly comparable to the conventional ship resistance tests familiar to naval architects. There is a reasonably well-defined distinction between resistance of a ship (which can be determined by a traditional bare-hull resistance test) and the propulsion generated by the propeller, which can be found by a propeller test. The interaction between the two, whilst of importance in ship design, is relatively small. In the case of a structure swimming with forward speed, such as the simplified eel, the two are completely inseparable and there is no significant meaning to the resistance or the propulsive thrust. All that can meaningfully be considered is the difference of the two. At zero forward speed, of course, the mean thrust may be found. Nonetheless, it is sometimes useful to consider a reference value of the resistance for the sake of comparison; in this case, some researchers have considered the condition in which the swimming structure is aligned with all sections parallel to the flow. This is sometimes referred to as the “stretched straight” condition.

5.1. Single-flapper zero speed tests

A series of eleven tests were carried out as “single flapper” tests. These were all based on a 30 degree oscillation with varying frequency. The goal of these tests was to develop an understanding of the performance of the model and the testing

methodology in the simplest realistic flow case, to examine how simple tests such as these could be used to derive the added mass and drag coefficients required for the simple Morison-based model, and to examine how well the simplified model can predict the various parameters for interest. The test is effectively equivalent to a “bollard-pull” test and is of practical interest in that the forces generated at rest will influence initial acceleration.

In order to determine the number of oscillation cycles over which the eel was run, the mean thrust was calculated on a cycle-by-cycle basis over a large number of runs and the convergence examined. It was found that there was some scatter in the data; however the mean value appears well-defined. The scatter relates to many factors, including the motion control, the hydrodynamics and the measurement system. In some of the very low frequency tests, for which the mean thrust is extremely small no such mean value is apparent and these results were discarded. Based on this study, a standard value of 30 oscillations was chosen; however in every case the convergence was examined and checked to ensure that the results were well-behaved.

The results of the tests are shown in Fig. 10. Results are broadly as might be expected; as frequency increases, with constant amplitude of oscillation, the cross-flow velocity increases linearly and the cross-flow acceleration increases quadratically. Consideration of Eq. (4) thus suggests that it is reasonable to expect that the mean force will increase approximately quadratically with frequency.

5.2. Modelling of “single-flapper” case zero speed tests using the Morison-based approach

The data shown in Fig. 10 can be used in conjunction with Eq. (4) to derive a set of force coefficients for this swimming case, through a standard process of linear least-squares fitting of the data. All points were equally weighted. An alternative was tried in which higher weighting was given to points with a larger absolute

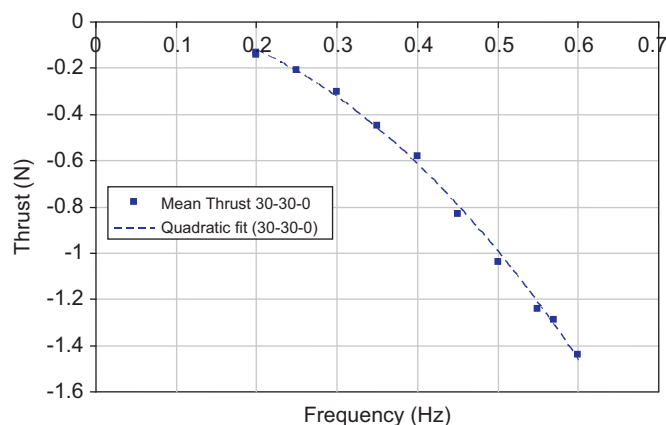


Fig. 10. Model test results for 30-30-0 "single flapper" case.

value, but it was found to increase the root-mean-square error in the time series.

In a simple application of Morison's equation, such as the prediction of force around a two-dimensional cylinder in an oscillating flow, the force coefficients are derived from measurements of force normal to the structure. In the current study, the relatively complex motion of the structure results in a net hydrodynamic force which varies in magnitude and direction through the cycle of motion. This force is decomposed into longitudinal and transverse components, both for the purposes of measurement and for the analysis of propulsion. In this simplified model, both components of force are assumed to result from the same mechanisms; hence it is reasonable to assume that both longitudinal and transverse force data should be used in the derivation of the force coefficients. Where both force components are used, the components may be weighted differently in the least squares fit in order to increase or reduce the influence of one force relative to the other.

However it is also possible to derive the coefficients solely from consideration of one component of the net force. It can be argued that consideration of the longitudinal force component alone might yield better prediction of the propulsive performance of the eel than consideration of both force components. In the current study three approaches were tried. In the first approach, the coefficients were derived from a combination of both force components with data scaled to give equal weighting to X-force and Y-force data; in the second approach, derivation was based only on the longitudinal force. Finally, for completeness, in the third approach, the coefficients were found by consideration of only the transverse force.

Two approaches were tried for handling data analysis given that more than one data set is available. In the first case, the coefficients were calculated individually for each run and an average value was calculated; in the second case the time histories were concatenated and a single calculation performed overall the resulting time values. One source of difference between these approaches stems from the different length of data records between tests; the sampling frequency was kept constant throughout at 213 Hz and each test ran for 30 cycles. Hence if all tests are concatenated there are more points contributed to the concatenated record from the low-frequency tests than from the high-frequency tests.

All permutations of these possibilities were tried; naturally different values of force coefficients were obtained. The difference between the two approaches for handling the multiple data sets was small, affecting the inertia coefficients by no more than 4%. The relative differences between coefficients gained based on the choice of force data used were quite large, especially for the inertia coefficient which is relatively small.

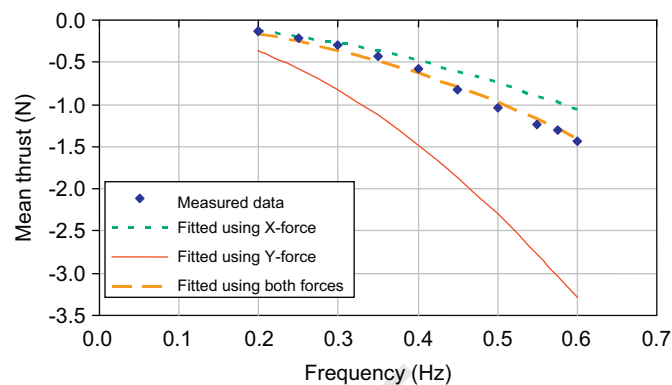


Fig. 11. Reconstruction of mean thrust from the Morison equation using different approaches for "single-flapper" case.

One comparison of particular interest is that between the mean thrust predicted using the derived coefficients and that measured in the tests. Over the frequency range considered, the better of the two predictions for mean thrust given by each of the three force fits is shown in Fig. 11. In this graph it should be noted that the mean thrust is positive left to right, but the eel is swimming right to left—hence this represents forward propulsion.

The approach using both transverse and longitudinal forces to derive force coefficients clearly gives the best overall fit to the measured data for mean thrust. This resulted in values of $C_a=0.37$, $C_d=4.45$, leading to a satisfactory fit over the frequency range. The prediction of mean thrust from the derivation based on longitudinal force alone yields better agreement with experiment data at lower frequencies, where the mean forces are small and rather less satisfactory fit at higher frequencies, where the mean forces are larger.

It can thus be seen that the mean forces are predicted reasonably well over a range of different frequencies by suitable derivation of force coefficients based on an appropriate fit to the force time history for this simple kinematic case. However, it is clearly possible that the quality of fit for force in one direction could be improved at the expense of some degradation of the quality of fit for the force in the other direction. Since the mean value of the force is relatively small compared to the maximum and minimum instantaneous values in the time history, even some quite subtle changes in the force coefficients can lead to relatively large changes in the mean values. This is presumed to be the reason for the particularly poor prediction of mean thrust in the case for which coefficients are derived from a fit only the transverse component of force alone. Since both components of force result from the same flow phenomena, it is reassuring that the use of both components to derive the coefficients from the force time histories leads to the best prediction for the mean thrust.

Unfortunately, comparison between the time histories predicted using the derived coefficients, indicate that the predictions of instantaneous forces do not fit the measured data as well as the predictions for mean thrust. The example shown in Fig. 12 is based on the best fit for mean thrust. The angle of the eel is indicated at a notional scale in order to indicate the phase of the forces. The root-mean-square error in the predicted data expressed as a percentage of the measured data is around 35% for the transverse force and around 38% for the longitudinal force. This indicates that the Morison equation is failing to capture all of the physics of the flow correctly. The Morison equation implicitly assumes locally two-dimensional flow normal to the body. The poor prediction of the time history of the forces is presumed to be

related to one or more of three factors: the assumption of constant force coefficients over the body of the eel, the neglect of effects related to tangential flow, or key three-dimensional effects related to flow near the tail.

In an attempt to improve this modelling, a more sophisticated version of Morison's equation was implemented. It is well-known that force coefficients are sensitive to the Keulegan–Carpenter number. Graham (1980) suggested through a theoretical approach that the coefficients could be expressed as

$$C_D = AK_c^{(3-2\lambda)/(2\lambda-1)}$$

$$C_m = C_{m0} + BK_c^{2/(2\lambda-1)} \quad (7)$$

In this equation the value λ depends upon the internal angle of the vortex-shedding edge. For a sharp thin edge such as found on a thin flat plate, $\lambda=2$. The constants A and B can be determined by numerical calculation or physical measurement. For a thin flat plate Graham estimated $A=11.8$ and $B=0.25$ using the discrete vortex method and found $A=8.0$ and $B=0.2$ from 2D U-tube measurements. The coefficient C_{m0} is the added mass coefficient for the body when flow is attached. For a thin plate – or the eel

with fins – it can reasonably be argued that the flow is never attached and that $C_{m0}=0$.

Following this argument, it is reasonable to suggest that the drag coefficient might depend upon the inverse cube-root of the Keulegan–Carpenter number, though it should be noted that Graham pointed out that empirical evidence suggested that the dependence might be closer to an inverse square root. The Keulegan–Carpenter number varies substantially along the length of the eel; in the case of the single flapper, K_c varied linearly from just over zero at the forward joint to just over one hundred at the tail in these trials.

Hence a second exercise was conducted in order to see if any improvement could be made by allowing the coefficients to vary as

$$C_D = AK_c^{-1/3}$$

$$C_m = BK_c^{2/3} \quad (8)$$

and using the least-squares fit to find the constants of proportionality A and B . Numerical computation using the results gave values of $A=7.47$ and $B=0.14$, slightly less than the values of $A=8.0$ and $B=0.2$ found by Graham for a flat plate.

However, using these values lead in practice to little improvement in either the mean thrust prediction or the root-mean-square error in the time histories. One example is shown in Fig. 13. It can be seen that the KC-dependent approach fits slightly better at the lower frequency and slightly less well at the higher frequencies.

It should be noted however that since the moments in the joints were not measured in these trials, then the distribution of force along the segment is unknown; it is possible that this distribution might have been better predicted using the KC-dependent coefficients.

5.3. Double-flapper zero speed tests

The second set of tests explored the effect of differing amplitude and phase of the rear segment over a range of frequencies. Two swimming patterns were investigated; in the first the oscillation amplitudes were identical in both segments and in the second the aft segment had a larger oscillation amplitude. In each case three frequencies were tested, over a range of phase angles. Results for mean thrust are shown in Fig. 14.

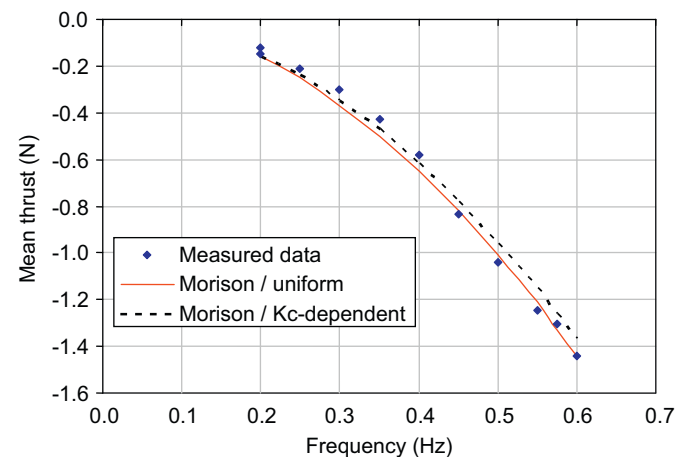


Fig. 13. Reconstruction of "single-flapper" mean thrust for 30-30-0 case using KC-dependent force coefficients.

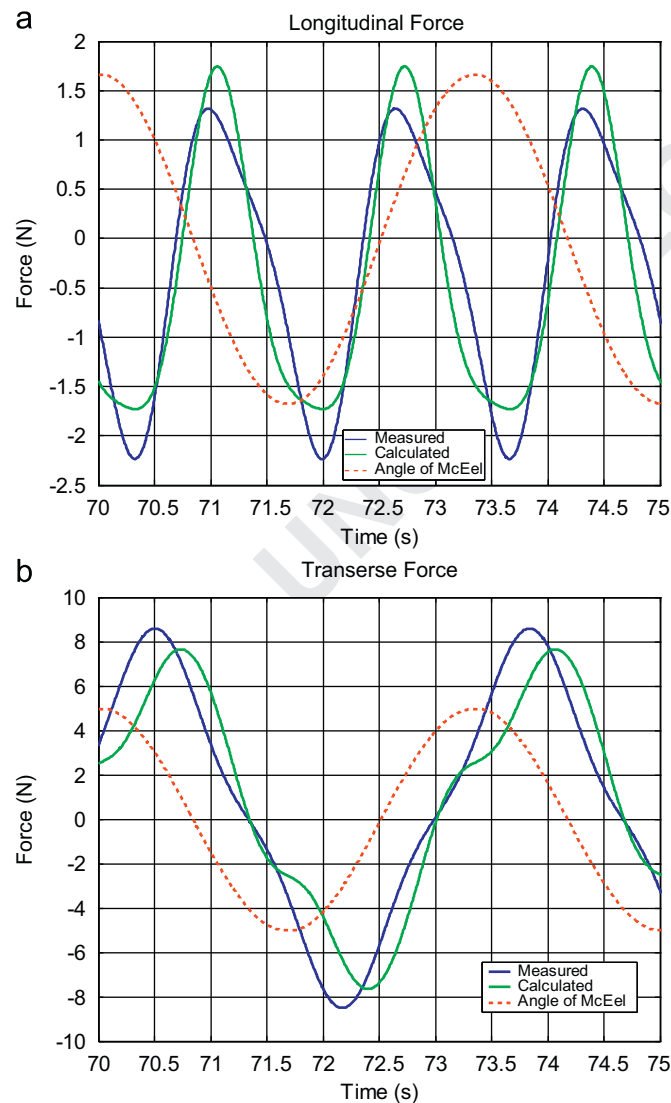


Fig. 12. Reconstruction of time history of forces using the Morison equation for "single-flapper" case.

Several observations can be made from these results. As expected from the single-flapper case, the mean thrust increased with increasing frequency. In each case the pattern with larger amplitude in the rear segment generated more mean thrust than the equivalent case with equal amplitudes in both segments. Finally it can be seen that the maximum thrust occurred with the oscillation of the second segment at a relative phase angle of around 30–40 degrees.

5.4. Modelling of zero-speed “double-flapper” case using the Morison-based approach

The data shown in Fig. 14 was used to recompute the values of the constants A and B in Eq. (8) using the forces in both longitudinal and transverse directions in a manner similar to that adopted for the single-flapper case. The added mass coefficient B remained constant at 0.14, but the best fit results showed the drag constant A dropping to from 7.47 to 5.87. Unfortunately in this case the mean thrust was not so well-predicted by the Morison-based approach. This is illustrated for one of the worst cases – the 30-40-60 test – in Fig. 15.

The root-mean-square error in the time histories is also considerably worse in the longitudinal direction than in the single-flapper case. This suggests that the simple Morison-type model starts to breakdown substantially as the phase difference between the motion of the forward and aft segments increases. This is illustrated in Fig. 16, in which it is seen that the error grows at a rate approximately proportional to the phase difference between the segments.

One key difference between the cases is the introduction of a tangential velocity component in the “double flapper” case, which is not present in the “single-flapper” case. Various attempts were made to improve the prediction by incorporating a tangential drag term into the model, but none were successful in substantially improving predictions.

5.5. Double-flapper forward speed tests

In the final set of tests, all of the swimming patterns which had been tested with zero forward speed were retested with a range of forward speeds. These were selected to ensure that some tests resulted in net positive thrust whilst others resulted in net negative thrust. A curve was then fitted to the data; a typical example is shown in Fig. 17. Once the effect of the sting was accounted for the point of zero net thrust was found—which is the mean speed which should be obtained for the self-propelled eel.

It can be seen that the points lay very close to a straight line allowing the speed to be predicted with confidence. It should be

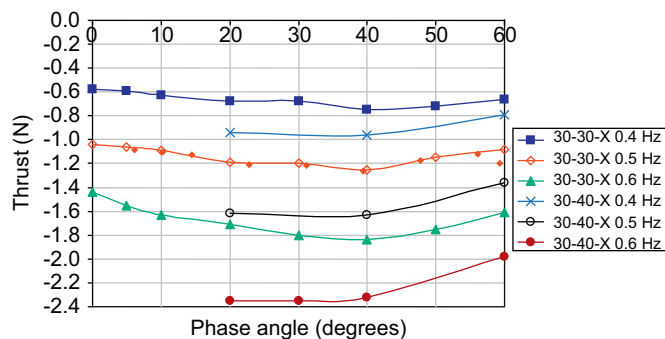


Fig. 14. Variation of zero-speed mean thrust with phase for different swimming patterns.

noted that the self-propulsion speed is higher than the speed at the point at which the line crosses the x-axis due to the resistance of the sting.

Since the previous results indicate that the higher frequency would naturally lead to higher thrust, four styles are compared for the same frequency of 0.6 Hz in Fig. 18. This indicates that the style with increasing amplitude towards the tail and the larger phase angle attains the highest self-propulsion speed. It is interesting to note by comparing the results from Fig. 18 and Fig. 14 that the 30-40-60 pattern, which produced the highest self-propulsion speed produced less mean thrust at zero speed than the 30-40-30 pattern. A similar observation may be made regarding 30-30-60 and 30-30-30. This suggests that for

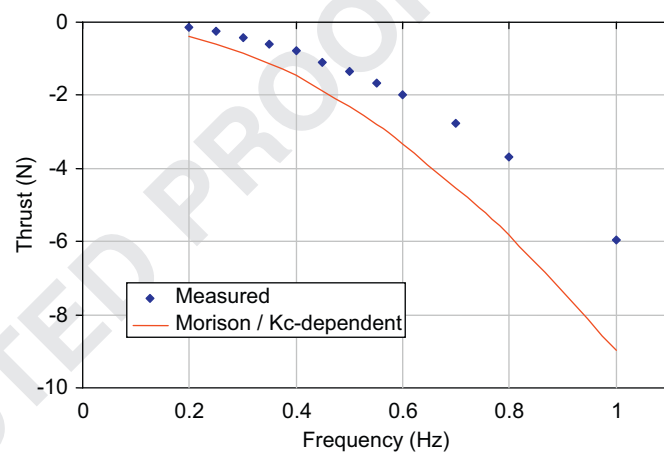


Fig. 15. Reconstruction of zero-speed mean thrust for 30-40-60 pattern using KC-dependent force coefficients.

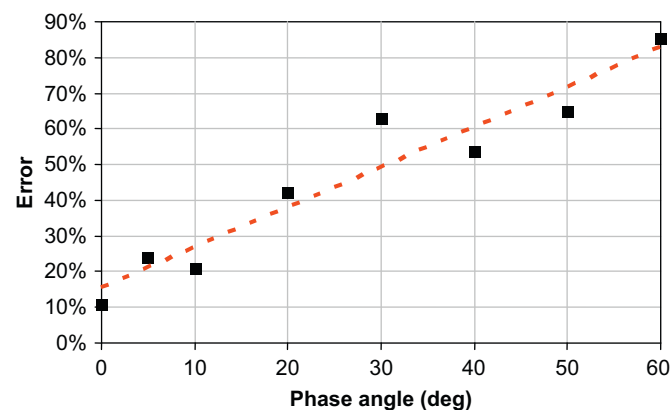


Fig. 16. Variation in mean-thrust error with phase angle.

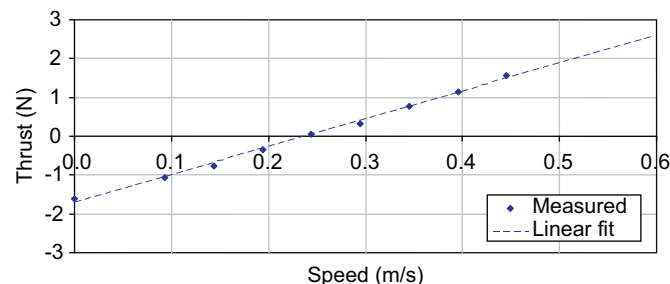


Fig. 17. Variation of thrust with speed (30-30-60, 0.6 Hz).

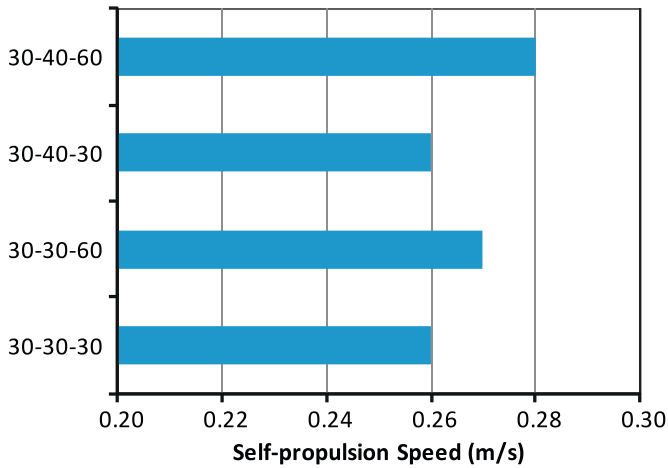


Fig. 18. Self-propulsion speed for different swimming patterns at 0.6 Hz.

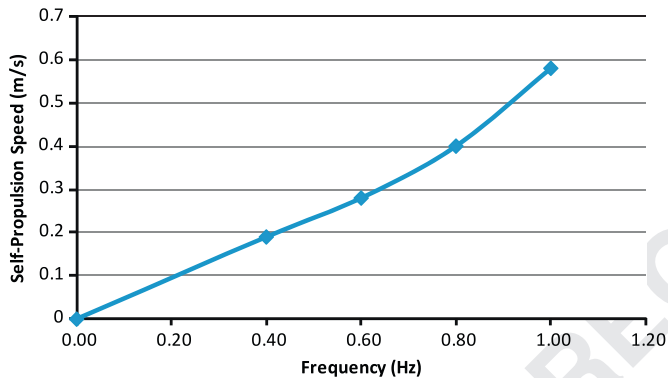


Fig. 19. Variation of self-propulsion speed with oscillation frequency.

maximum performance the phase angle of the rear segment should increase as the speed increases.

The effect of oscillation frequency on the fastest swimming style is shown in Fig. 19. As might be expected from the variation of mean thrust at zero speed, the self-propulsion speed increased with increasing frequency; the variation is approximately quadratic.

5.6. Modelling of zero-speed "double-flapper" case using the Morison-based approach

The final calculation examined the possibility of predicting the self-propulsion speed of the eel using the Morison-based approach. The model described previously only predicts the mean thrust and makes no attempt to capture the resistance. It was therefore assumed that the resistance of the eel could be obtained from the data in the straight position as described in Section 4.2. A series of calculations is then carried out over a range of speeds in a manner analogous to the experiment test procedure and the predicted self-propulsion point obtained. This process is illustrated in Fig. 20 for the 30-40-30 case. Perhaps surprisingly, the errors in the predicted speed are rather less than the errors in the mean thrust.

The variation of self-propulsion speed with frequency predicted by the Morison-based approach for the 30-40-60 case is compared with the measured data in Fig. 21. In this case the worst error for self-propulsion speed is 21%. For all the swimming styles

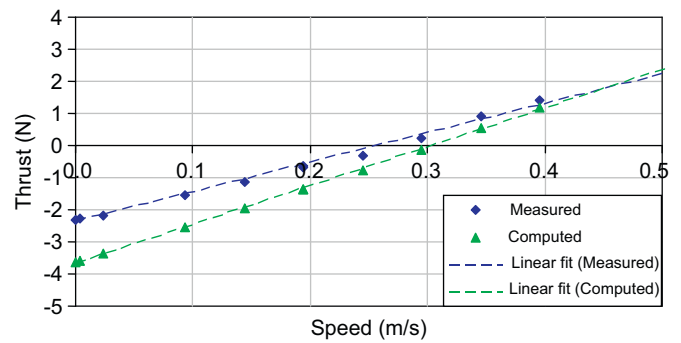


Fig. 20. Prediction of self-propulsion speed using the Morison-based approach (30-40-60, 0.6 Hz).

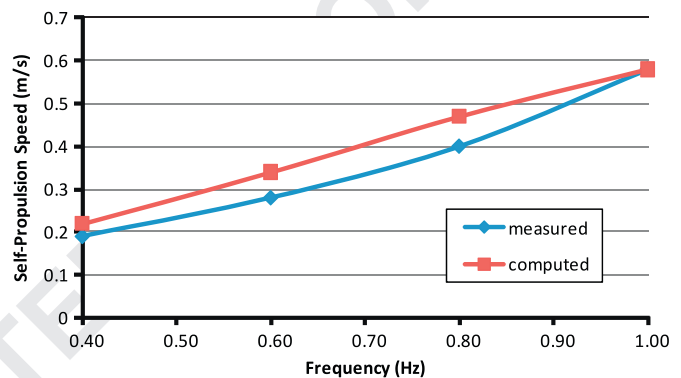


Fig. 21. Computed variation of self-propulsion speed with frequency using the Morison-based approach for 30-40-60 style.

tested, the worst error found was 29%. All computed values were found to over-estimate the speed.

5.7. Comparison with data from real eels

It is interesting to compare the results obtained from these tests with data from measurements of real eels. A detailed study of the motion of the American Eel both on water and on land is presented by Gillis (1998). Four individuals were studied, with length between 0.35 and 0.39 m, compared with the total length of the structure presented here of 0.81 m. Gillis characterized speed in terms of body lengths (L) advanced per second; studies in water were carried out between 0.4 and 1.0 L/s .

With regard to the kinematics of the eel body, Gillis noted that at the lower speeds the forward half of the body underwent no significant lateral undulations; whilst at higher speeds the proportion which was laterally stationary reduced to one third. For the mechanical eel, the forward 51% of the body underwent no oscillations; hence it can be seen that the proportion of the structure which is non-oscillatory in the lateral direction is consistent with the real eel. The extent of the lateral displacement at the tail tip, however is rather different. Gillis found a maximum lateral tail-tip displacement of 0.08 L , compared to a maximum value of 0.25 L for the mechanical eel in the 30-40-60 pattern. However, it is interesting to note that the slope of the body of the real eel near the tail is comparable at both low and high speeds to the 40 degree value, which provided the fastest eel propulsion speeds in the model tests. It is thus possible that the requirement for relatively large transverse displacements in the model results from the relatively crude discretisation of the oscillating part of the eel into two segments of equal length. It should also be noted that other similar-sized elongated swimmers, including snakes and salamanders, swimming at similar speeds, exhibit tail-tip

amplitudes in the range from 0.11 to 0.19 (see for example Jayne, 1985, Gillis, 1997).

The speed range for self-propulsion of the mechanical eel is in the range between 0.25 and 0.75 L/s, which is slightly lower than the range of the real eels. Gillis showed that the relationship between speed and frequency is approximately linear for real eels, with oscillation frequency varying between around 1.0 Hz at low speeds and 2.5 Hz at the high speeds. This was based on observations at three speeds with a reasonable degree of scatter. The Strouhal number of the flow (based on length) thus remains approximately constant, varying between 0.96 and 0.98. In contrast, the results for the mechanical eel (see Fig. 19) indicate a slightly non-linear variation of speed with frequency over the range studied (0.4–1.0 Hz), yielding a Strouhal number variation between 1.4 and 1.7. However, it should be noted that the swimming pattern of the real eel changes with the speed, whereas the results for the mechanical eel show the variation of speed with frequency for the same swimming pattern, so the two sets of results are not strictly comparable.

In summary it can be seen that many of the trends exhibited by the tests of the mechanical eel broadly reflect the behavior of real eels, although there are some clear differences, which can be attributed at least in part to the substantial simplification of the geometry in the mechanical eel.

6. Discussion and conclusions

Computation of hydrodynamic forces generated by fish- (or eel-) like motions is a challenging problem for many reasons including the substantial changes of the body geometry through the swimming cycle. The decomposition of forces in a manner traditional in ship design, into components related to resistance and propulsion is not particularly meaningful in the context of a fish-like vehicle.

Computation of the performance of a simplified mechanical eel-like device is arguably more challenging than for a realistic motion due to the discontinuities at the joints. The motion of the mechanical eel generates velocities and accelerations both perpendicular and tangential to the segments. Previous simplified approaches to prediction of forces on such structures have neglected either inertia or drag forces. In the current study a simplified approach based on the Morison equation was investigated to explore how well it can predict longitudinal and transverse forces. The method allows calculation of both drag and inertia forces, but required input of the associated force coefficients. Two versions were developed, with both the Keulegan–Carpenter number dependent and independent coefficients.

A physical model of a three-segment mechanical eel was designed, built and tested in a towing tank. The model was used to examine the swimming performance of a simplified eel in three modes: the zero-speed “bollard-pull” case with the two oscillating segments moving as if rigidly joined to simulate a single oscillating segment, designated as the “single-flapper” approach; the zero-speed case with two oscillating segments, and a large set

of runs with forward speed and two oscillating segments. It was shown that greater performance at both zero-speed and self-propulsion speed resulted from the use of two segments with the aft segment oscillating at a larger angle than the forward section and with a phase lag relative to the forward section. The data suggests that for maximum performance, the phase lag should be greater at self-propulsion speed than at rest. The mean thrust at zero speed and the self-propulsion speed increase approximately quadratically with oscillation frequency.

A series of comparisons were made between the model test data and the predictions from the simplified Morison-based approach with force coefficients derived from the test data. The mean thrust was quite well-predicted for the zero-speed “single-flapper” case, although the time histories indicate that instantaneous forces are less well-predicted. However when the segments move independently, the error in the zero-speed mean thrust prediction increases as the phase difference between the segments increases; it can reasonably be argued that the effect of changing the phase angle is to amplify existing deficiencies in the assumptions made in the Morison equation, and/or to introduce or exaggerate hydrodynamic effects not accounted for, such as vortex shedding at the tail. Nonetheless, perhaps surprisingly, the simplified method was found to estimate the self-propulsion speed to within 30% in all the cases examined.

References

- Azuma, A., 2006. The Biokinetics of Flying and Swimming, second ed. American Institute of Aeronautics & Astronautics.
- Breder, C.M., 1926. The locomotion of fishes. *Zoologica* 4, 159–297.
- Carling, J., Williams, T.L., Bowtell, G., 1998. Self-propelled anguilliform swimming: simultaneous solution of the two-dimensional Navier–Stokes equations and Newton’s laws of motion. *J. Exp. Biol.* 201 (23), 3143–3166.
- Gawn, R.W.L., 1950. Fish Propulsion in Relation to Ship Design. *Trans. R. Inst. Nav. Archit.*
- Gillis, G.B., 1997. Anguilliform locomotion in an elongate salamander (*Siren intermedia*); effects of speed on axial undulatory movements. *J. Exp. Biol.* 200, 767–784.
- Gillis, G.B., 1998. Environmental effects on undulatory locomotion in the American eel *anguilla rostrata*: kinematics in water and on land. *J. Exp. Biol.* 201, 949–961.
- Graham, J.M.R., 1980. The forces on sharp-edged cylinders in oscillatory flow at low Keulegan–Carpenter numbers. *J. Fluid Mech.* 97 (2), 331–346.
- Gray, J., 1936. Studies in animal locomotion–VI. The propulsive powers of the dolphin. *J. Exp. Biol.* 13, 192–199.
- Jayne, B.C., 1985. Swimming in constricting (*Elaphe g. guttata*) and nonconstricting *Nerodia fasciata pictiventris* Colubrid snakes. *Copeia* 1985 (1), 195–208.
- Lighthill, M.J., 1960. Note on the swimming of slender fish. *J. Fluid Mech.* 9 (2), 305–317.
- Lighthill, M.J., 1971. Large-amplitude elongated-body theory of fish locomotion. *Proc. R. Soc. Lond. B* 179, 125–138.
- McIsaac, K.A., Ostrowski, J.P., 2003. Motion planning for anguilliform locomotion. *IEEE Trans. Robotics Autom.* 19 (4), 637–652.
- Morison, J.R., O’Brien, M.P., Johnson, J.W., Schaaf, S.A., 1950. The force exerted by surface waves on piles. *Pet. Trans.* 189, 149–154.
- Singh, K., Pedley, T.J., 2008. The hydrodynamics of flexible body manoeuvres in swimming fish. *Physica D* 237, 2234–2239.
- Triantafyllou, M.S., Barrett, D.S., Yue, D.K.P., Anderson, J.M., Grosenbaugh, M.A., Streitlien, K., Triantafyllou, G.S., 1996. A new paradigm of propulsion and maneuvering for marine vehicles. *Trans. SNAME* 104, 81–100.
- Triantafyllou, M.S., Techet, A.H., Zhu, Q., Beal, D.N., Hover, F.S., Yue, D.K.P., 2002. Vorticity control in fish-like propulsion and manoeuvring. *Integr. Comp. Biol.* 42, 1026–1031.
- Videler, J.J., 1993. Fish swimming (*Fish and Fisheries*, no. 10), First ed. Springer.